A three-dimensional kinematic analysis of tongue flicking in *Python molurus*

Jurriaan H. de Groot[1,*], Inke van der Sluijs[1], Peter Ch. Snelderwaard[1] and Johan L. van Leeuwen[2]

[1]*Section Evolutionary Morphology, Institute of Biology (IBL), Leiden University, PO Box 9516, 2300 RA Leiden, The Netherlands* and [2]*Experimental Zoology Group, Wageningen Institute of Animal Sciences (WIAS), Wageningen University, Marijkeweg 40, 6709 PG, Wageningen, The Netherlands*

*Author for correspondence (e-mail: j.h.de_groot@lumc.nl)

Summary

The forked snake tongue is a muscular organ without hard skeletal support. A functional interpretation of the variable arrangement of the intrinsic muscles along the tongue requires a quantitative analysis of the motion performance during tongue protrusion and flicking. Therefore, high-speed fluoroscopy and high-speed stereo photogrammetry were used to analyse the three-dimensional shape changes of the tongue in *Python molurus bivittatus* (Boidae). The posterior protruding part of the tongue elongated up to 130% while the flicking anterior portion elongated maximally 60%. The differences in tongue strains relate to the absence or presence, respectively, of longitudinal muscle fibres in the peripheral tongue. Maximum overall protrusion velocity (4.3 m s^{-1}) occurred initially when the tongue tip left the mouth. Maximum tongue length of ~0.01 body length (20 mm) was reached during the first tongue flick. These observations are discussed within the scope of the biomechanical constraints of hydrostatic tongue protrusion: a negative forward pressure gradient, longitudinal tongue compliance and axial tongue stiffness. The three-dimensional deformation varied along the tongue with a mean curvature of 0.06 mm^{-1} and a maximum value of 0.5 mm^{-1}. At the basis of the anterior forked portion of the tongue tips, extreme curvatures up to 2.0 mm^{-1} were observed. These quantitative results support previously proposed inferences about a hydrostatic elongation mechanism and may serve to evaluate future dynamic models of tongue flicking.

Key words: snake, tongue, tongue sheet, muscular hydrostat, flicking, curvature, 3-D kinematics, high-speed fluoroscopy, X-ray.

Introduction

Snakes and some other squamates use forked tongues for chemo- and mechanoreception (Schwenk, 1994, 1995; Bels et al., 1994). During a probing action, the tongue protrudes, oscillates (flicks) while collecting airborne and substrate-fixed chemical particles and subsequently retracts (Ulinski, 1972; Gove, 1979). In the mouth, chemicals are transported to and stimulate the vomeronasal organ (e.g. Meredith and Burghardt, 1978; Bertmar, 1981; Gillingham and Clark, 1981; Young, 1990; Schwenk, 1994, 1995). The pattern of tongue flicking is related to external stimuli, such as the presence of prey or predators, and involves behavioural and seasonal aspects (e.g. Chiszar et al., 1976, 1977; Gove, 1979; Graves and Halpern, 1990; Bels et al., 1994).

The mechanisms of tongue protrusion and superimposed tongue flicking in snakes are still poorly understood. The intrinsic and extrinsic muscles involved were identified by morphological studies (Gnanamuthu, 1937; Hershkowitz, 1941; Frazzetta, 1966; Langebartel, 1968; Kier and Smith, 1985; Smith and Mackay, 1990), electromyographical recordings (Meredith and Burghardt, 1978; Smith, 1984, 1986; Herrel et al. 1998) and kinematic observations (Smith, 1984, 1986; Bels et al. 1994; Herrel et al. 1998). In contrast to several other squamate taxa, snake tongues lack hard skeletal support.

Instead, the tongue behaves like an almost incompressible muscular hydrostat (cf. Kier and Smith, 1985) with interesting similarities to the highly extensible muscular tentacles in squid (van Leeuwen and Kier, 1997). Muscle fibre activation leads to complex distributions of fibre forces and fluid pressures that 'drive' the deformations in the tongue. A quantitative analysis of the tongue is challenging due to complex connective tissue and muscle fibre arrangements, highly non-linear mechanical tissue properties and very large deformations.

The protruding tongue must satisfy three important mechanical demands. First, a negative longitudinal pressure gradient is required in the tongue, similar to that in an extending squid tentacle (Van Leeuwen and Kier, 1997); second, a sufficiently high axial stiffness to prevent excessive bending; third, enough longitudinal compliance to accommodate the extreme overall elongation of ~100% (Smith, 1984). Superimposed tongue flicking requires precisely controlled spatial variations in axial compliance and bending moments.

To understand the mechanical contribution of the tongue muscles in terms of forces and work, and consequently tongue architecture, a number of steps is proposed (as summarised by Van Leeuwen et al., 2000) that include (1) the measurement of
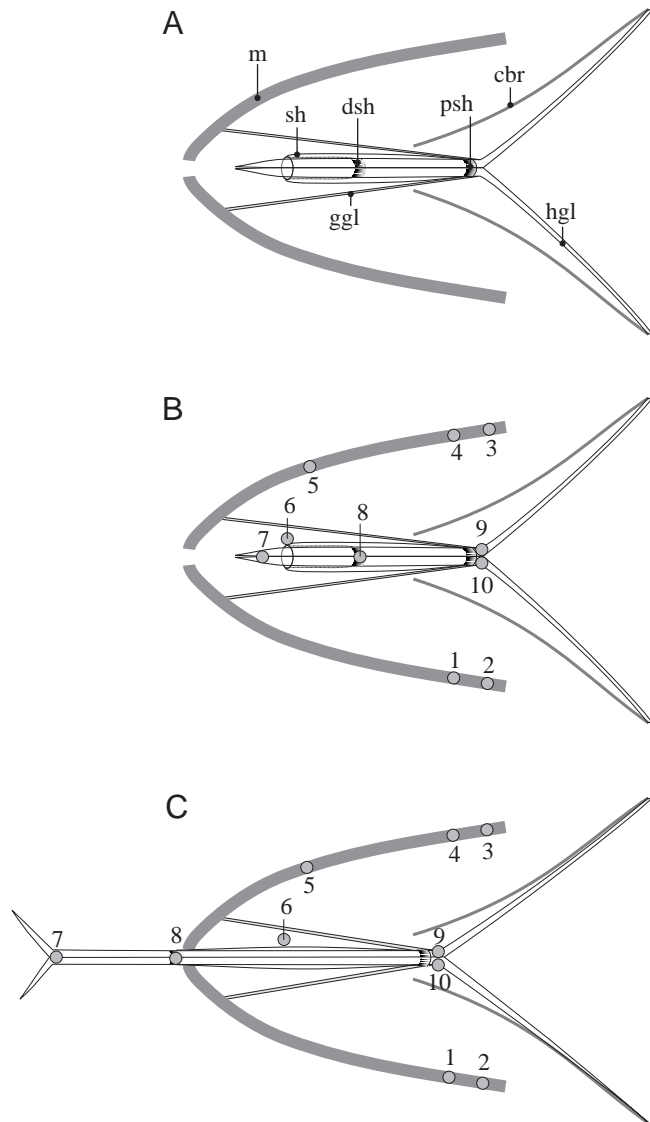
Fig. 1. Schematic dorso-ventral representation of the tongue of *Python molurus* and its extrinsic muscles. (A) Abbreviations: cbr, ceratobranchial; m, mandible; dsh, distal tongue ensheathing; ggl, m. genioglossus; hgl, m. hyoglossus; psh, proximal tongue ensheathing; sh, tongue sheet. The dental bone forms the local coordinate system of the head. Although the head is highly deformable during feeding, the lower jaws do not deform during tongue flicking. The position of the ceratobranchials is assumed to be fixed to the skull during tongue flicking (e.g. Bels et al., 1994). The mm. genioglossi and the mm. hyoglossi are able to protract and retract the tongue relative to the mandibles and ceratobranchials. Proximally on the tongue, the mm. hyoglossi are ensheathed. This tubular tongue sheet encloses the tongue distally up to the tongue tips, inverts into itself and connects to the tongue at the distal tongue ensheathing (McDowell, 1972). The outer tongue sheet is connected to the muscles and connective tissue of the mouth floor. The inverted inner part is protruded while the tongue elongates. (B) Radio-opaque marker positions at rest: 1–5, local coordinate system fixed (glued) to the jaws (skin); 6, fold of the tongue sheet at maximum tongue retraction – the outer layer of the tongue sheet is fixed to the connective tissue of the mouth floor; 7, point of bifurcation (marker injected); 8, proximal tongue ensheathing (marker glued after manual protrusion of the tongue); 9, 10, tongue base (markers injected). (C) Hypothetical displacements of the markers indicating the relative translation and elongation of the soft tissues.

from forward dynamic simulations (e.g. Chiel et al., 1992; Van Leeuwen and Kier, 1997; Van Leeuwen, 2002).

We applied two techniques to record the tongue kinematics of the Burmese python (*Python molurus bivittatus*). The deformation of the whole tongue was recorded by high-speed fluoroscopy (Snelderwaard et al., 2002). The 3-D kinematics of the protruded and flicking tongue that extends out of the mouth was obtained by high-speed photogrammetry developed for the recording of spatial soft-tissue deformation (de Groot and Van Leeuwen, 2002). First, a general description of the tongue morphology and muscle function is presented to facilitate understanding of the experimental procedures, kinematic analysis and functional interpretation.

Tongue morphology

The snake tongue, schematically represented in Fig. 1A, can be divided into three portions: (1) the distal bifurcated tongue tips, (2) an anterior portion of the tongue, which protrudes out of the mouth during tongue flicking, and (3) a posterior portion of the tongue that remains almost entirely within the mouth during protrusion (Smith and Mackay, 1990). The tongue is suspended in the floor of the mouth by a folded tongue sheet that is dorsally stiffened by the larynx and trachea (McDowell, 1972). The origin of the tongue sheet attaches at the posterior end of the tongue body and inserts at the transition between the anterior and the posterior portions of the tongue (Fig. 2A). In the fully retracted tongue, the 'outer sheet' covers the complete tongue (Fig. 2B). Anteriorly, the sheet folds inward and forms a second 'inner sheet'. The inner sheet covers the anterior portion of the retracted tongue. When the tongue is fully extended, the sheathing is completely unfolded and

the architecture and tissue properties, (2) the development of a quantitative model that predicts the optimal design of the system and (3) the acquisition of experimental data for comparison with model predictions. A spatial forward-dynamics model of snake tongue is currently being developed (Van Leeuwen, 2002) that accepts microscopic data on tongue morphology (Smith and Mackay, 1990) and material properties of the tissues as input.

In the present paper, we quantify the forward translation and internal elongation of the whole tongue body, i.e. from the proximal tongue ensheathing to the point of bifurcation (Fig. 1), and distinguish between the contribution of the posterior portion of the tongue and the anterior (extended) portion of the tongue. We quantify the mechanical behaviour of the tongue during flicking, in particular its protrusion and spatial kinematics. The selected kinematic variables such as local tongue acceleration, velocity and position and the changing 3-D shape of the tongue are similar to those derived
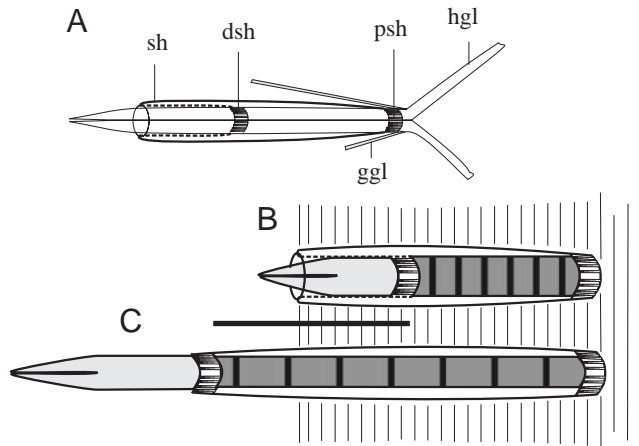
Fig. 2. Schematic representation of the longitudinal deformation of the tongue body and the interaction with the tongue ensheathing. The extrinsic muscles are only partly drawn. Abbreviations: dsh, distal tongue ensheathing; ggl, m. genioglossus; hgl, m. hyoglossus; psh, proximal tongue ensheathing; sh, tongue sheet. (A) Detail from Fig. 1A. The tongue sheet is a tubular structure that inserts the tongue body at the proximal and distal ensheathing, thus forming a loose second 'skin' around the tongue body. (B) In the retracted 'rest' position, the tubular sheet distally folds inward, resulting in a double sheathing along the tongue tip. The outer layer of the tongue sheet is fixed to the connective tissue of the mouth floor (as indicated by the thin vertical lines). (C) While the tongue protrudes, the inner sheet unfolds outward as the posterior tongue part, i.e. between the proximal and distal ensheathing, elongates and the distal tongue part is revealed. Thus, the tongue sheet forms an almost frictionless bearing for tongue protrusion.

envelops only the outer surface of the posterior portion of the tongue (Fig. 2C; McDowell, 1972; J. H. de Groot and I. van der Sluijs, personal observations). Only the outer sheet is connected to the floor of the mouth and allows the posterior portion of the tongue to elongate freely, without straining the connective tissues of the mouth floor.

The major tongue muscles, the paired m. hyoglossus, originate from the posterior part of the external tongue skeleton, i.e. the cartilaginous hyoids. The individual muscles converge in a V shape, 'enter' the tongue and extend along the entire length of the tongue while keeping their separate identity (Hershkovitz, 1941; Langebartel, 1968; McDowell, 1972; Smith and Mackay, 1990). The mm. hyoglossi continue into the tongue tips. Activation of the extrinsic posterior portion of the mm. hyoglossi generates retracting forces on the whole tongue body. Activation of the intrinsic mm. hyoglossi tends to shorten the tongue locally due to the longitudinal arrangement of the muscle fibres. Spatial left–right asymmetry of the intrinsic longitudinal muscle fibre activation results in lateral bending forces.

The antagonists of the extrinsic part of the mm. hyoglossi are the mm. genioglossi, originating from the dentary bone and inserting into the posterior part of the outer sheathing (Frazzetta, 1966; Langebartel, 1968; McDowell, 1972). Activated mm. genioglossi generate protracting translation forces on the tongue

base, preventing the tongue base of the elongating tongue from moving posteriorly (cf. chameleon tongue projection; Herrel et al., 2000; de Groot and Van Leeuwen, in press) and contributing to the forward tongue translation.

The muscle fibre distribution in the anterior portion of the tongue differs from the posterior portion (Hershkowitz, 1941; Kier and Smith, 1985; Smith and Mackay, 1990). A transverse section of the posterior portion of the tongue reveals the paired longitudinal mm. hyoglossi, the transversal m. verticalis and m. transversus and the circumferential m. circularis (Kier and Smith, 1985; Smith and Mackay, 1990). In the anterior portion also, dorsal longitudinal bundles are found (Hershkovitz, 1941; Smith and Mackay, 1990). Contraction of the circumferential and transverse muscles results in a tongue diameter decrease and, due to the incompressible character of the muscular hydrostat, tongue elongation (Kier and Smith, 1985; Chiel et al., 1992). The combined antagonist contraction of the longitudinal muscle fibres of the mm. hyoglossi and dorsal longitudinal muscles results in the shortening of the tongue body. Dorso-ventral bending of the anterior tongue depends on the contractile state of the mm. hyoglossi and the dorsal longitudinal muscles, in combination with gravitational forces (Smith and Kier, 1989).

Electromyographical (EMG) recordings in snakes (Meredith and Burghardt, 1978) and other tongue-flicking squamates (Smith, 1984; Herrel et al., 1998) indicated an involvement of the mm. genioglossi during protraction and the mm. hyoglossi during subsequent retraction. Activation of intrinsic tongue muscle fibres was recorded in combination with tongue kinematics (mm. hyoglossi, m. circularis) during tongue protrusion of *Tupinambis* and *Varanus* during feeding. Intrinsic longitudinal straining of more than 100% coincided with the activity of m. circularis (Smith, 1984, 1986).

Materials and methods

Tongue flicking of *Python molurus bivittatus* Kuhl 1820 (female, snout–vent length=2.0 m, body mass=4 kg, 1.5 years of age) was recorded with a high-speed digital video camera (Kodak SR-500, resolution: 512×480 pixels) and three mirrors to obtain synchronous images of the tongue from four different viewpoints on every video frame (Fig. 3). The 3-D position of the tongue axis was estimated from the recorded images (de Groot and Van Leeuwen, 2002). The internal translations and deformations of the tongue were recorded by high-speed fluoroscopy (Snelderwaard et al., 2002). Prior to the motion recording, the python was not fed for two weeks. The local ethical committee (U-DEC 98022) approved all experiments.

In the following, the tongue is defined as the non-bifurcated portion of the tongue body. The motions of the tongue tips were not quantified.

High-speed fluoroscopy

Surgically inserted radio-opaque (lead) markers helped to identify the positions of relevant landmarks of the tongue. High-speed X-ray fluoroscopy of these markers allowed us to
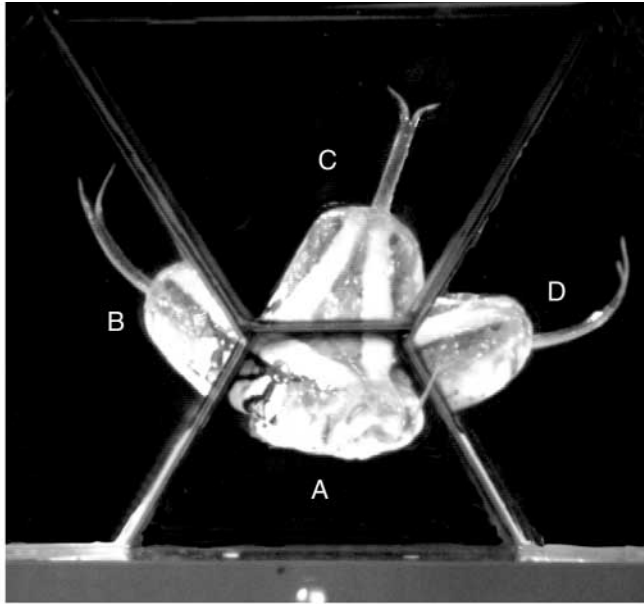
Fig. 3. Camera frame of *Python molurus* during a tongue flick (Kodak SR-500; resolution 512×480 pixels). Four images were recorded synchronically by the use of three supplementary mirrors, resulting in: (A) frontal image (direct camera view); (B) right lateral image (mirror); (C) dorsal image (mirror); (D) left lateral image (mirror).

measure the separate contributions of whole tongue translation and length changes of the tongue to protrusion and retraction. The python was instrumented under complete anaesthesia (200 ml min^{-1} of 1.5% isofluoran, 135 ml min^{-1} N$_2$O). The chosen marker locations (Fig. 1B) were based on careful dissections of preserved and freshly frozen specimens of *Python molurus bivittatus* and related species (*Python sebae*, *Python regius* and *Boa constrictor constrictor*). The markers were either glued on or injected into different structures of the tongue system. The glued markers were disk-shaped (height≈0.2 mm, ∅≈1 mm) and glued onto the head (markers 1–4), onto the jaw (5), onto the mouth floor just adjacent to the distal insertion of the tongue sheet to the floor of the mouth (6) and, after manual protraction of the tongue, onto the posterior ensheathing, adjacent to the proximal insertion of the tongue sheet (8). The injected markers were cylinder-shaped (length≈1 mm, ∅≈0.3 mm) and inserted into the point of bifurcation of the tongue (marker 7) and into the mm. hyoglossi through an incision in the skin (9, 10).

The instrumented python was placed into a plastic (Plexiglas) tunnel (1 m×0.3 m×0.3 m) that could be moved relative to the X-ray camera system. Lateral images of the tongue at 250 frames s^{-1} (shutter 1/3000 s) were stored by recording the X-ray fluoroscopy image of the internal image intensifier with a high-speed digital camera (Kodak Motion Analyzer SR-500, resolution 512×480 pixels; Snelderwaard et al., 2002). Only tongue flick sequences with long tongue lengths and performed in the mid-sagittal plane of the head (within approximately 15°) were selected for analysis, thus

minimising 2-D projection artefacts due to lateral curving of the tongue. Selection was instantly made through visual inspection. After each successful recording, a perforated metal plate was recorded in the plane of the tongue flick. The grid image was used to calibrate the image (scaling and correction of image deformation) by means of a custom-made computer programme. Finally, nine recordings were selected, and the positions of all markers were digitised. The positions of markers 6–10 were expressed in the head-fixed coordinate frame using markers 1–5. The position (x) of the radio-opaque markers and their mutual longitudinal distances (l) were determined in two tongue positions: the initial position at rest (x_0, l_0) and at maximum tongue protrusion with the tongue straight in front of the mouth (x_m, l_m). Subsequently, the tongue translation relative to the head, $d=(x_m-x_0)$, and maximum tongue strain, $\varepsilon_{max}=(l_m-l_0)/l_0$, were calculated.

3-D motion analysis

The python was placed in a plastic tunnel of 1.0 m×0.3 m×0.3 m. At one end of the tunnel, a 'collar' of three mirrors was placed with an opening that just fitted the head of the python. The angle of the mirrors with the vertical frontal plane was ~45°. A high-speed digital camera (Kodak Motion Analyzer SR-500, resolution 512×480 pixels) was placed at ~1 m in front of the opening.

The python was lured to put her head through the opening with rat scent on cotton wool. Once through the hole, the head and the exposed tongue were projected by the three mirrors (Fig. 3). In each camera frame, four images of the head and tongue were obtained: frontal (A), right lateral (B), dorsal (C) and left lateral (D), resulting in four synchronous projections of the 3-D position of the tongue relative to the head. The parameters that relate the image coordinates to 3-D positions were calibrated by direct linear transformation (DLT; see Woltring and Huiskes, 1990). This resulted in 11 DLT parameters per image that were valid for all subsequent frames of a tongue-flick event due to the fixed positions of camera and mirrors.

Three tongue-flick sequences were recorded at 250 frames s^{-1}. Assuming symmetry along the central axis of the tongue, the 3-D position of the central axis of the tongue could be derived from the contours of the tongue projections. The method used here was described in detail elsewhere (de Groot and Van Leeuwen, 2002).

For each recorded frame, the coordinates of the finite 3-D tongue axis, i.e. from mouth opening to the point of bifurcation, were described by a third-order polynomial curve. This curve was defined by a coefficient vector $P=(a_0, a_1, a_2, a_3, b_0, b_1, b_2, b_3, c_0, c_1, c_2, c_3)$ and variable s. For each value of $0{\leq}s{\leq}1$ and for the given P-coefficients, a unique combination of x, y and z coordinates was defined (e.g. Van der Helm et al., 1992):

$$x = a_0 + a_1s + a_2s^2 + a_3s^3 \text{ for } s \in [0,1]\,, \tag{1}$$

$$y = b_0 + b_1s + b_2s^2 + b_3s^3 \text{ for } s \in [0,1]\,, \tag{2}$$

$$z = c_0 + c_1 s + c_2 s^2 + c_3 s^3 \text{ for } s \in [0,1] \, . \qquad (3)$$

Each of the four images recorded in one frame was calibrated by means of 11 DLT parameters and resulted in a unique mathematical relationship between the 2-D projections and the 3-D coordinates. Thus, for each combination of 2-D image coordinates (u, v), a spatial 3-D position (x, y, z) could be calculated and *vice versa*. The position of the tongue axis was estimated by calculating the single combination of P-coefficients for which the projection of the 3-D tongue axis $[x(s), y(s), z(s)]$ optimally fitted the recorded and digitised projections of the central tongue axis (u, v) in each of the four images in the frame. This optimal fit was obtained by application of a simplex optimisation routine. This procedure was repeated for each recorded frame. Thus, for each frame of the recorded tongue-flick sequence, a set of 12 P-coefficients was obtained. For n frames, the result is a time trace of $n \times 12$ coefficients. Finally, the time trace of each coefficient was filtered (25 Hz low-pass recursive Butterworth filter), which resulted in a mathematical 3-D description of the tongue axis for a complete tongue flick.

The P-coefficients (and thus the local x, y and z coordinates of the central tongue axis) were calculated in the coordinate system of the calibration frame. The coordinates were subsequently expressed in the local coordinate system of the snake head with the x-axis as the longitudinal axis of the mid-sagittal plane, i.e. from caudal to rostral, the y-axis as the vertical axis of the mid-sagittal plane, i.e. from ventral to dorsal, and the z-axis as the right lateral axis, i.e. from medial to the right-hand side.

From the 3-D description, we derived the external protrusion length by integration along the longitudinal axis for each recorded image from the mouth opening to the bifurcation point of the tongue. Protrusion velocity and acceleration were obtained from the first and second time differential of the external length trace. Tongue curvature, C (= 1/radius), along the axis was numerically determined from 51 points along the tongue axis for $s = (0, 0.02, \ldots, 1)$ (equations 1–3). A circle with radius r and centre M was numerically calculated for each set of three contiguous points along the tongue axis (Fig. 4).

The 3-D time trace or trajectory of the bifurcation point of the tongue during the flick was obtained from equations 1–3 for $s = 1$. The velocity and acceleration in the three coordinate directions were obtained from the first and second time differential of the position of the bifurcation point.

Results

High-speed fluoroscopy

The movements of the tongue portion that resides in the mouth are not externally visible. However, high-speed fluoroscopy of radio-opaque markers allowed a quantitative distinction between the contributions of whole tongue translation and tongue elongation to protrusion (Fig. 1B,C). The presented results are based on nine recordings. The length of the tongue axis was derived only from the position of the
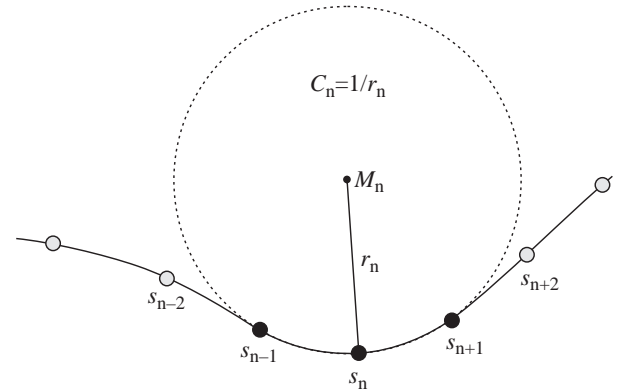

Fig. 4. Schematic representation for the calculation of tongue curvature. The solid line, including seven discrete points, represents a digitised section of the tongue. A circle with radius r and centre M is stepwise estimated along the tongue through each set of three contiguous points along the tongue axis, e.g. the three black dots s_{n-1}, s_n and s_{n+1} [i.e. for $s = (0, 0.02, 0.04, \ldots, 1)$; equations 1–3]. Subsequently, at s_n, the curvature C (i.e. $1/r$) was determined. This was repeated for each point at the tongue axis except for the tongue base ($s = 0$) and tongue tip ($s = 1$).

markers in the selection of frames where the tongue was protruded linearly in front of the mouth (for instance, marker 7 in Fig. 1B,C is straight in front of the mouth). The displacements and deformations of the tongue were expressed along the posterior–anterior x-axis. The posterior boundary of the tongue was defined by the mean position of the two markers inserted into the mm. hyoglossi (markers 9 and 10; Fig. 1). Marker 7 indicated the anterior boundary of the tongue.

The tongue positions and translations relative to the 'fixed' marker at the mouth floor (marker 6; Fig. 1) and lengths and deformations are summarised in Table 1. The initial position of the tongue in the mouth varied with a standard deviation (S.D.) of 16.6 mm. The initial tongue length (≈ 25 mm) was almost constant (S.D.$= 0.54$ mm). The maximum tongue length showed a large variation, as reflected by the high S.D. The general variation will even be higher as we made a selection of tongue flick clusters based on direction and sufficient length. The forward tongue translation, i.e. the average displacement of markers 9 and 10 in the mm. hyoglossi, was 5.3 ± 0.99 mm. This translation is controlled by external muscle forces and was denoted as the whole tongue translation. The posterior end of an elongating tongue would tend to move caudally in the absence of such forces. The total tongue protrusion was, on average, more than 110% of the initial tongue length: ~10% originated from tongue translation and ~100% from tongue elongation. The elongation of the tongue was not uniformly distributed. The mean longitudinal strain of the posterior portion of the tongue, defined by $\varepsilon_{post} = \Delta l_{post}/l_{0,post}$, was 1.28, while the mean longitudinal strain of the anterior portion, defined by $\varepsilon_{ant} = \Delta l_{ant}/l_{0,ant}$, was 0.60.

Three-dimensional high-speed photogrammetry

The 3-D motion of the longitudinal tongue axis was derived

Table 1. *Mean tongue position (mm), translation (mm) and deformation (%), recorded by high-speed fluoroscopy*

		INIT (mm)	MAX (mm)	DIF (mm)	REL (%)
M. hyoglossus:	(#9+#10)/2	−80.1±16.61	−74.8±17.05	5.3±0.99	10.8±0.5%
Anterior tongue:	#7–#8	11.0±0.35	17.7±1.24	6.7±1.32	60.5±13.0%
Posterior tongue:	#8–(#9+#10)/2	13.9±0.55	31.6±1.69	17.9±1.48	128.0±12.5%
Total tongue:	#7–(#9+#10)/2	24.9±0.54	49.3±2.32	24.5±2.45	98.0±10.6%

The marker numbers #7–#10 coincide with the numbers in Fig. 1. Means ± S.D. are given for N=9 different tongue flick sequences.

INIT, the initial (rest) position of the tongue (m. hyoglossus markers) and initial tongue length (mm); MAX, the position of the tongue (m. hyoglossus markers) and tongue length at maximum protrusion (mm); DIF, displacement of the tongue (m. hyoglossus markers) and tongue elongation from the initial position to maximum protrusion (mm); REL, displacement of the tongue (m. hyoglossus markers) and tongue elongation from the initial position to maximum protrusion expressed as a percentage of the initial tongue length.

Table 2. *Summary of the temporal and spatial protrusion characteristics of the tongue axis*

Cluster number	Number of flicks	Protrusion duration (s)	Max. protrusion (m)	Max. protrusion velocity (m s^{-1})	Max. protrusion acceleration (m s^{-2})	Mean curvature ± S.D. (mm^{-1})	Max. curvature (mm^{-1})
1	3	0.60	0.020	0.314	20.1	0.061±0.068	0.44*
2	2	0.46	0.019	0.431	8.8	0.065±0.072	0.49*
3	2	0.42	0.016	0.439	9.0	0.055±0.046	0.39*

*During the final flick of each of the flick clusters, high curvatures of 1.5 mm^{-1} up to 2.0 mm^{-1} were recorded at the transition of the tongue (body) and the tongue tips. These data were not included in the analysis for this table.

Table 3. *Summary of the kinematics of the bifurcation point*

Cluster number	Covered distance (m)	x-velocity (m s^{-1}) Min.	Max.	y-velocity (m s^{-1}) Min.	Max.	z-velocity (m s^{-1}) Min.	Max.	x-acceleration (m s^{-2}) Min.	Max.	y-acceleration (m s^{-2}) Min.	Max.	z-acceleration (m s^{-2}) Min.	Max.
1	0.113	−0.30	0.29	−0.54	0.71	−0.06	0.12	−33.7	22.0	−42.9	34.7	−5.7	6.7
2	0.069	−0.27	0.16	−0.30	0.39	−0.09	0.05	−16.6	11.6	−15.4	16.4	−5.5	3.5
3	0.081	−0.25	0.40	−0.47	0.42	−0.06	0.12	−26.0	20.1	−33.4	19.7	−7.8	8.9

for three tongue-flick clusters. The 3-D analysis was necessarily restricted to the externally visible protruded portion of the tongue. The duration of a flick cluster, defined from the moment that the tongue tips appeared to the moment that they disappeared, was 0.60 s for the first cluster of three flicks, 0.46 s for the second cluster and 0.42 s for the third cluster.

The tongue tips made a remarkable 'clapping' motion at the early appearance of the tongue. The two tongue tips were slightly apart initially. Subsequently, the tips adducted maximally, abducted and adducted again prior to the appearance of the point of bifurcation. After this double 'clapping' motion, the tongue tips finally abducted and separated for the full duration of the flicking cluster. The motion of the bifurcated tongue tips was not further included in the quantitative 3-D analysis.

The 3-D description of the tongue position allowed the analysis of the kinematics along the longitudinal axis of the tongue, i.e. tongue length, protrusion velocity and protrusion acceleration

(Table 2), and the 3-D kinematics of the tongue in the global coordinate system, i.e. the trajectory, velocity and acceleration of the bifurcation point and tongue curvature (Tables 2, 3). The maximum external tongue length ranged between 16 mm and 20 mm. The maximum protrusion velocity was observed at the moment of appearance of the tongue body (Fig. 5) and ranged between 0.31 m s^{-1} and 0.43 m s^{-1}. The maximum tongue length was reached at the first downward flick in each of the three flick clusters (Fig. 5). The tongue tips in the first and second cluster touched the ground during this initial flick.

The trajectory and kinematics of the bifurcation point were derived from equations 1–3 for s=1, and the 3-D shape of the tongue was determined every 4 ms for $0 \leq s \leq 1$. The tongue axis was visualised from three mutually perpendicular viewpoints, e.g. lateral, frontal and dorso-ventral (Fig. 6). The velocity and acceleration of the bifurcation point is shown in Fig. 7 and summarised in Table 3. The velocities and accelerations in the vertical y-direction were slightly higher than those in the
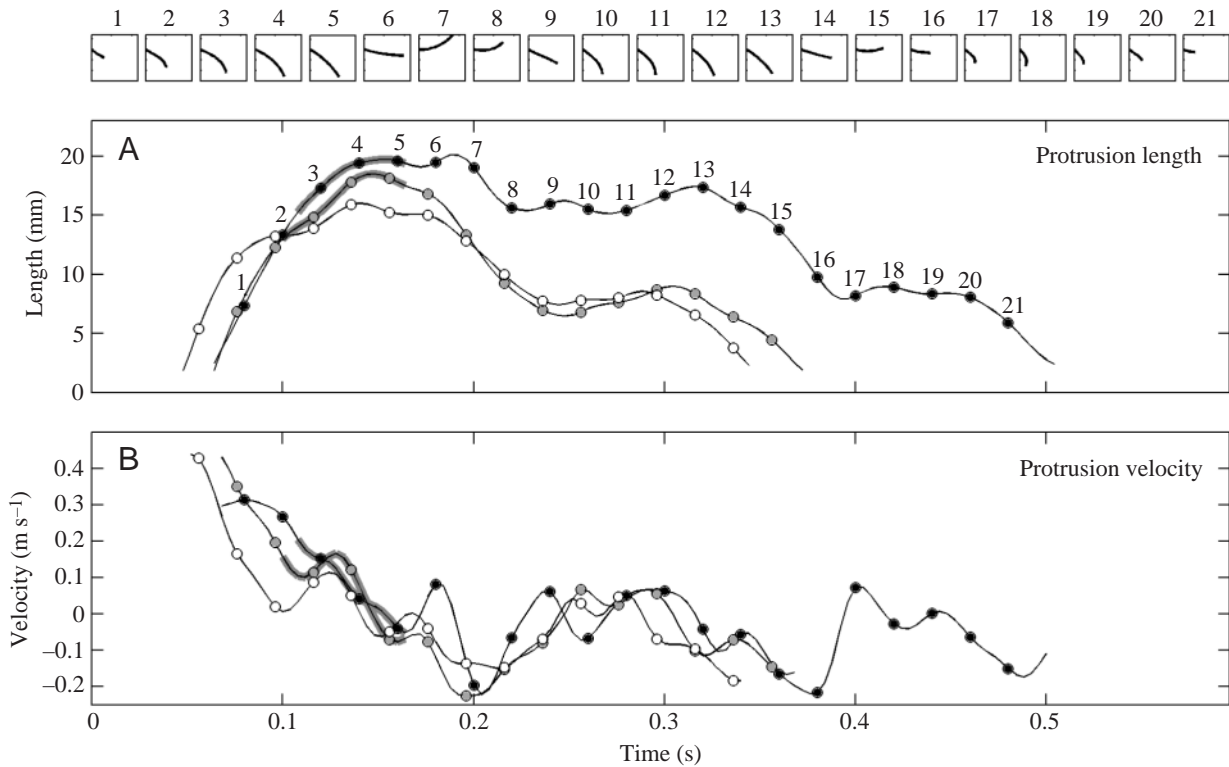
Fig. 5. Protrusion (A) and protrusion velocity (B) of *P. molurus* for three recorded tongue-flick clusters (cluster 1, black circles; cluster 2, grey circles; cluster 3, open circles). The clusters differ in duration and maximum protrusion length. The series of small panels at the top of the figure shows the tongue axis position (lateral view, tongue tip pointing to the right) of the protrusion trace with the longest duration (black circles). Each numbered panel corresponds to the same number in the position time trace. Protrusion length was calculated along the 3-D tongue axis from mouth opening to the bifurcation point of the tongue. At time $t=0$ s, the tips of the tongue started to become visible. Protrusion was started before the bifurcation point became externally visible, which explains the initial high protrusion velocity. The marked (grey) traces in flick clusters 1 and 2 indicate ground contact of the tongue tips.

horizontal *x*-direction. The selected tongue flicks remained close to the sagittal plane and resulted therefore in relatively low lateral velocities (± 0.1 m s^{-1}) and accelerations (± 5 m s^{-2}) in the *z*-direction. The time trace of the covered distance of the bifurcation point is assumed equivalent to the spatial exposure of the tongue, i.e. the amount of sampled air during the flicks (Fig. 8). The recorded traces show more or less the same slope for the three flicking sequences with a mean velocity of the bifurcation point of 0.25 m s^{-1} within a range of 0.04 m s^{-1} to 0.65 m s^{-1}. The covered distance of the bifurcation point was almost proportional to the total duration of the tongue flick. The maximum covered distance for each of the three flick sequences was 113 mm, 69 mm and 81 mm, respectively.

The curvature of the tongue was calculated at 49 equally distributed sections along the longitudinal axis for each recorded frame (Fig. 9). The curvature pattern differed for each of the clusters. The colours in the figure indicate the curvature according to the coded colour bar. The repeated red vertical striation in Fig. 9 coincides with an almost straightened tongue, which in time is followed by an increased curvature (yellow–green–blue). The straightened tongue did not necessarily point horizontally forward as illustrated in, for example, pictogram 4 (Fig. 9A) and pictogram 6 (Fig. 9B),

where the tongue was downwardly directed. In the initial phases of the first and second clusters, a ventral concavity at the tongue base and the distal tongue was observed, while the middle part was almost straight. In the initial phase of the third cluster, the tongue tip initially moved dorsally upward with a dorsal concavity. During the following downward stroke, the dorsal concavity of the tongue portion near the mouth remained while the distal portion curved ventrally, indicating an S shape along the tongue (Fig. 9C, pictogram 4). The final phase in all three clusters showed a similar pattern. During the last upward stroke, the distal portion is strongly curved ventrally while the portion near the mouth curves dorsally upward. During the final retraction, the distal tongue portion curved dorsally upward and subsequently disappeared into the mouth.

The tongue curvature, *C*, averaged along the tongue and for each of the flick clusters, was ~0.06 mm^{-1}, with a maximum curvature of ~0.5 mm^{-1} (Table 2). At the transition between the tongue and the tongue tips, however, the maximum curvature ranged from 1.5 mm^{-1} to 2.0 mm^{-1} during the final upward stroke. The tips made an angle with the more posterior tongue body of ~80°.

The motions of the tongue tips were not quantified. Here, we summarise some qualitative observations. During early
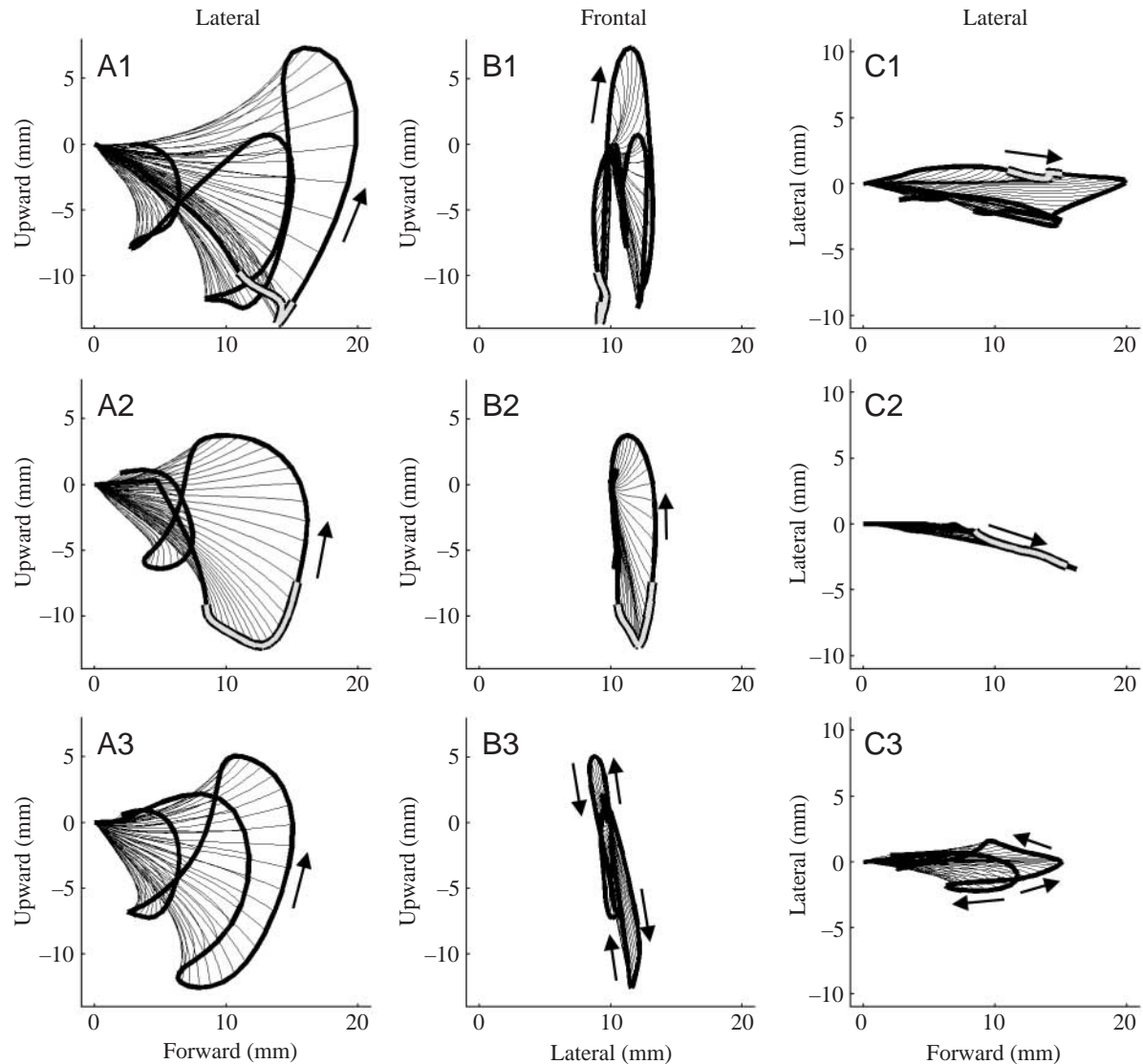
Fig. 6. The 3-D trajectory of the bifurcation point (thick trace) recorded at three different tongue flick clusters (rows 1–3) and for three different views: (A) lateral, (B) frontal and (C) dorso-ventral. The thin lines show the (calculated) position of the protruded part of the tongue axes for each recorded frame. The arrows indicate the motion direction of the bifurcation point. In the lateral view (A1–A3), the arrow coincides with the first flick within each of the clusters. The initial tongue flick started twice with a downward protrusion (clusters 1 and 2) and ground contact of the tongue tips (marked by light traces along the tongue tip trajectory) and once with an upward protrusion (cluster 3).

protrusion, the tongue tips made a repetitive abduction and adduction, or double 'clapping' movement, before separating. We could not discriminate whether this movement was a mechanical instability caused by the accelerating tongue or an intentionally controlled movement. During tongue flicking, the tongue tips moved relatively independently from the tongue and, in two flick sequences, the tongue tips touched the floor at the first downward oscillation (Figs 5, 6).

Discussion
Spatial and temporal tongue exposure in relation to behaviour

The tongue tips collect chemical particles and the tongue serves as the multidirectional 'carrier' for these tongue tips (Gove, 1979). The precise mechanism of collection of environmental chemical particles and the derivation of, for example, trailing parameters during tongue flicking (e.g. Schwenk, 1994) are still hypothetical. We assume that the success of particle collection is positively correlated with spatial and temporal exposure of the tongue, i.e. the distance covered by the tongue tip and the duration of tongue flicking. The aerodynamics may also play an important role in the success of particle collection. The relationship between these 'key events' of tongue exposure, particle collection and the transformation to trailing information, which are yet unknown, should be identified in order to understand the behavioural constraints of tongue flicking. Gove (1979) determined the spatial exposure
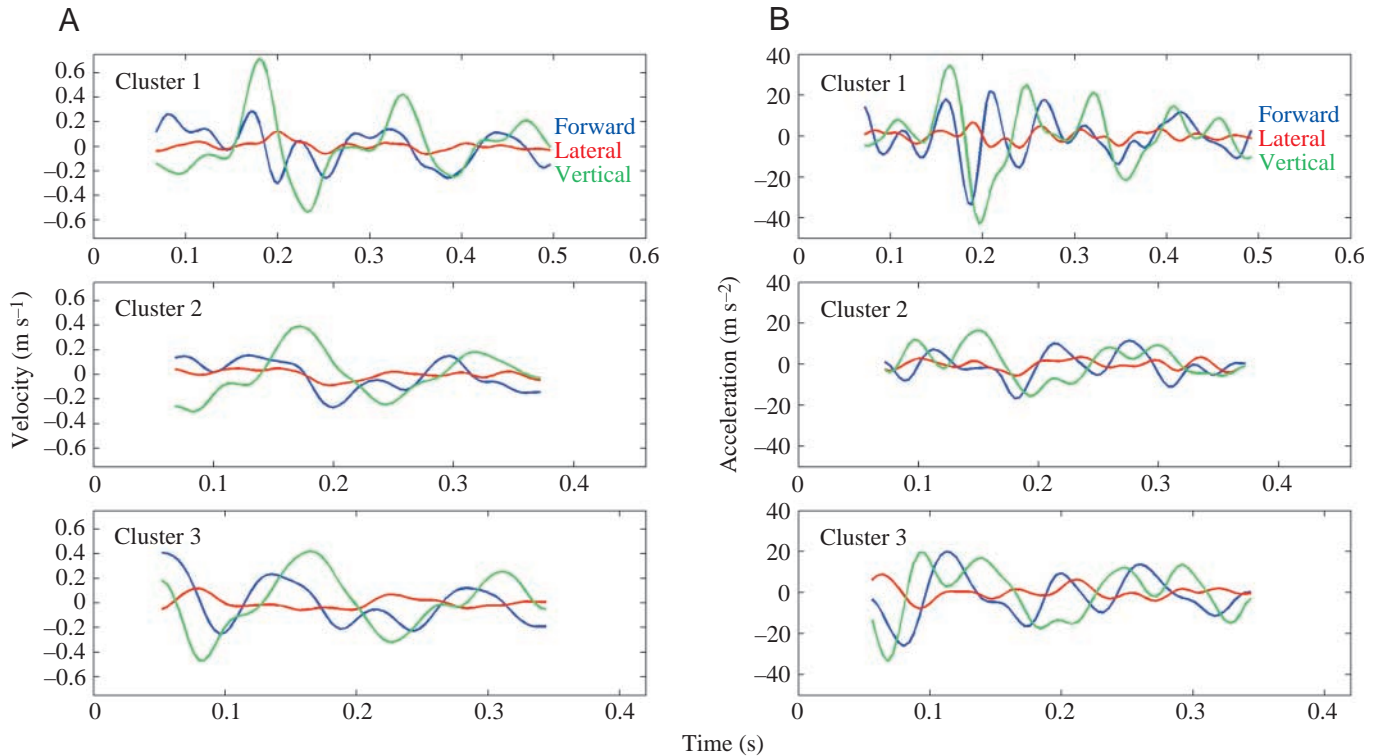
A

B

Fig. 7. (A) Velocity and (B) acceleration traces of the point of bifurcation of the tongue along the covered trajectory for the three tongue flick clusters shown in Figs 5, 6. The range of the time axis is chosen to represent the time interval that the tongue tips are visible for each of the three tongue flick clusters. The blue curve indicates forward velocity and acceleration, the red curve indicates lateral velocity and acceleration and the green curve indicates vertical velocity and acceleration.

relative to head size in two dimensions. The accuracy of the method was sensitive for motions deviating from the sagittal plane, and the absolute magnitude of tongue exposure was camouflaged and distorted by relating exposure to head size. Our three-dimensional approach allows the quantification of spatial exposure independently from the direction of tongue motion. The covered distance of the recorded tongue flicks ranged between 70 mm and 110 mm with a protruded tongue length of

15–20 mm. Simultaneously, the velocity of the tongue tip was derived. The 3-D motion analysis of the tongue tip (Fig. 8) revealed that the tip of the tongue is constantly in motion, which is in contrast to what might be concluded from a 2-D motion analysis. Tongue flicking is a combination of oscillations in three orthogonal directions, as illustrated in Fig. 7.

The mean resultant velocity vector, i.e. the average slope of the cumulative covered distance in Fig. 8, was ~0.25 m s^{-1} for the three tongue flick clusters analysed. The spatial and temporal exposure of the tongue seemed to be more or less linearly correlated for the observed flicks. The temporal exposure is a good predictor for the spatial exposure for these observed tongue flicks, i.e. three independent approaches, provoked by the same stimulus. For behavioural studies on a single specimen, the time of tongue exposure may turn out to be an easy to record parameter for spatial exposure. However, three tongue-flick clusters recorded from one specimen of python during an explorative type of behaviour are not sufficient for a definite conclusion.
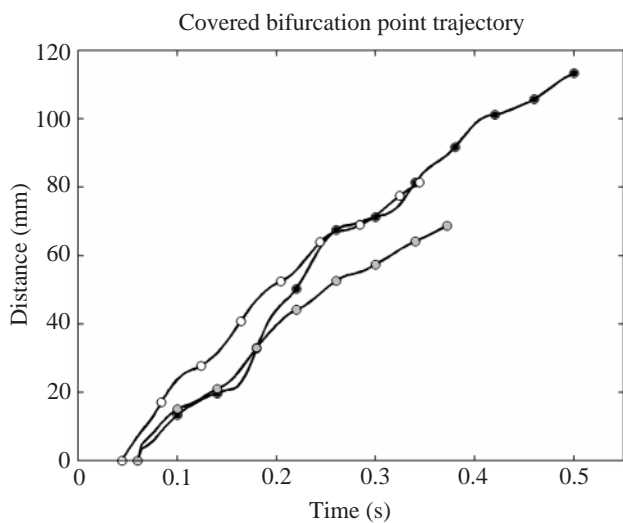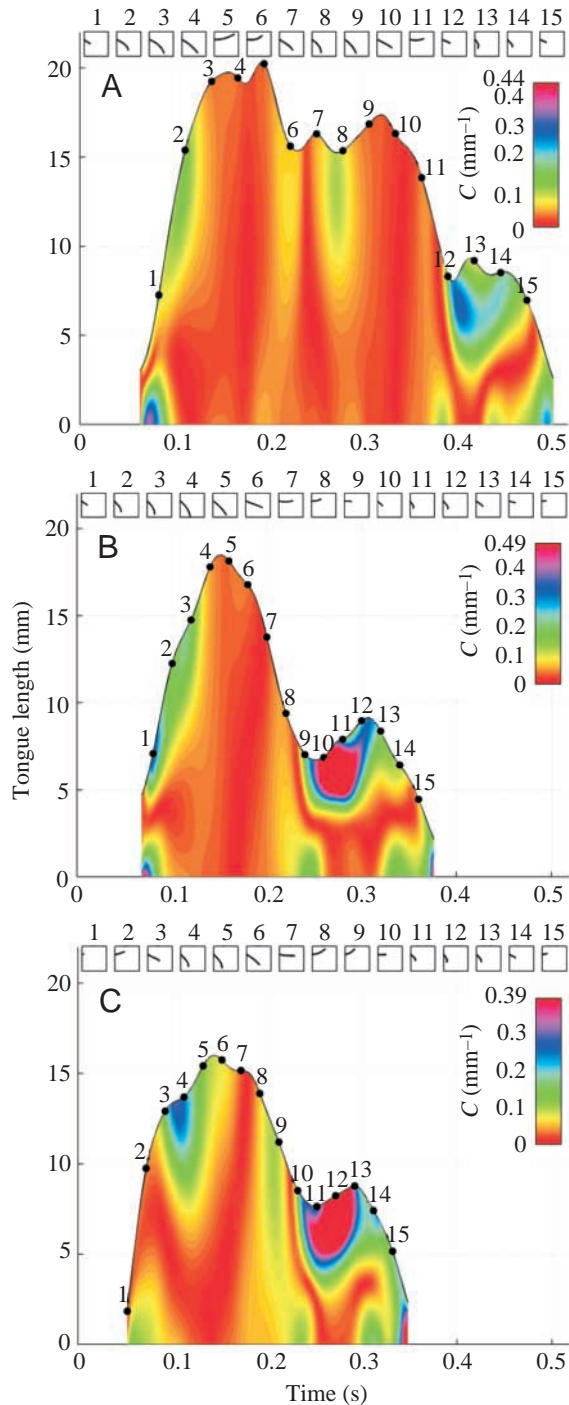

Fig. 8. Time trace of the covered distance of the bifurcation point during the three tongue flick clusters (1, black circles; 2, grey circles; 3, open circles) and indicating the spatial and temporal exposure of the tongue. The mean velocity (0.25 m s^{-1}) coincides with the overall slope of the curves. Numbering of flick clusters corresponds with Figs 5–7, 9.

Fig. 9. Tongue length (vertical amplitude) and tongue curvature along the tongue axis (colour code) through time (horizontal axis) for each of the first (A), second (B) and third (C) flick clusters. Numbering of flick clusters corresponds to those of Figs 5–8. The upper boundary of each plot represents the changing external tongue length (from the mouth to the bifurcation point; similar to Fig. 5A). Each vertical line under the curve represents the absolute curvature C (mm^{-1}) indicated by the colour code (see colour bar) along the tongue axis (mm) at a specific time (s). The numbered series of lateral tongue shapes in the small pictograms above each curve coincides with the numbered marks along the upper boundary. For instance, in A at recording 2 (0.1 s), the anterior portion of the tongue shows the highest curvature, indicated by the green area under the upper boundary. At recording 4 (0.17 s), the tongue is fairly straight, indicated by the orange area along the vertical axis (see also the lateral view of the tongue in pictogram 4).

Morphological and functional differentiation of the tongue

On the basis of observed morphological differences between the anterior and posterior portion of the tongue, Smith and Kier (1989) and Smith and Mackay (1990) proposed a functional differentiation in the tongue body. The design of the posterior portion of the tongue indicated an important contribution in tongue protrusion, while the asymmetrical arrangement of the longitudinal fibres in the anterior portion indicated an important role in flicking. Our high-speed fluoroscopic analysis of the tongue protrusion revealed 10% forward translation of the tongue and, simultaneously, 100% elongation of the whole tongue. The longitudinal strain in the tongue was non-uniformly distributed. The posterior portion elongated ~128% while the anterior portion elongated only 60%.

The tongue strains observed in *Python* and the strains reported in *Tupinambis* (Smith, 1984) are of the same order of magnitude. The gross tongue morphology of *Python* and *Tupinambis* also show correspondence. The proposed mechanism of hydrostatic elongation of tentacles and tongues (Kier and Smith, 1985; Smith and Kier, 1989) and illustrated by quantitative model simulations (Chiel et al., 1992; van Leeuwen and Kier, 1997) is likely to be at work in the tongue of the *Python*. Elongation of the tongue is realised by a decrease of the cross-sectional area of the tongue, induced by shortening of the transverse, vertical and circumferential muscle fibres in the tongue.

The exact role of the individual intrinsic muscle fibres during tongue flicking in the entire tongue and specifically in the anterior tongue portion is difficult to predict from our kinematic study. The gravitational and inertial components, in combination with the muscle forces, resulted in the observed tongue oscillations. Both concave and convex curvatures in the sagittal plane were simultaneously observed along the tongue axis (Fig. 9). During the tongue flicks, curvature waves travelled along the tongue in both forward and backward directions, indicated by the positive and negative slopes of the green (curved) and red (linear) areas in Fig. 9. The time traces of the oscillations of the bifurcation point were not symmetrical (Figs 6, 7). The local stiffness of the tongue along

The duration of tongue exposure, determined by Gove (1979) for 26 ophidian species, was minimally 100 ms with a mean duration of ~150 ms. Tongue exposure should be above a lower time limit, such that enough chemical particles are collected for an adequate sensory transmission. The duration will also be related to tongue length and flicking velocity (spatial exposure) and the sensory capacity of the vomeronasal organ. With the present 3-D recording technique we illustrate that it is now possible to quantify and combine these spatial and temporal requirements.

its axis is probably not constant but continuously adjusted by muscular activity. The exact nature of this control and the mechanical consequences cannot be derived from kinematics alone and need to be analysed by dynamic model simulations (e.g. van Leeuwen, 2002).

At the transition of the tongue to the bifurcated tongue tips, extreme curvatures of $1.5–2$ mm^{-1} were observed during the final upward motion of the bifurcation point in each of the three flick clusters (Fig. 9). Hydrostatic shortening requires a reduced tension in the circular muscles during retraction and, simultaneously, an increased tension in the retractors, which results in a lower bending stiffness of the tongue. The reduction of the length of the flicking tongue results in the redistribution of kinetic energy over a smaller tongue mass. The reduced vertical diameter of the tongue at the transition of the tongue body to the tongue tips in combination with the lower hydrostatic bending stiffness and the increase of kinetic energy may explain the extreme curvature during the final upward motion of the tongue tip.

The mechanism of tongue protrusion

In the Introduction, three demands on tongue protrusion were defined. For the optimal forward protrusion, (1) a negative forward pressure gradient was required in the muscular hydrostat; (2) sufficiently high stiffness was required to control bending amplitude and (3) enough longitudinal compliance was required to accommodate tongue protrusion. During protrusion, we observed a forward translation of the tongue that must have originated from the mm. genioglossi. The muscle compensated for the backward forces from the intrinsic tongue elongation and generated positive work. Electromyogram (EMG) activity of this muscle has indeed been demonstrated for tongue protrusion in snakes (Meredith and Burghardt, 1978) and other tongue-flicking squamates (Smith, 1984; Herrel et al., 1998).

The observed 130% elongation of the posterior portion of the tongue and the 10% superimposed forward translation leave no other conclusion but that a negative forward pressure gradient must have been generated in the muscular hydrostat. The negative forward pressure gradient is likely to be generated by the activation of m. transversus, m. verticalis and m. circularis and the simultaneous activation of the mm. genioglossi.

The second and third demand on the protruding hydrostat involved axial stiffness in combination with longitudinal compliance. In the snake tongue, the posterior portion of the tongue ejects the anterior portion of the tongue and the tongue tips. In mechanical terms, the posterior soft body pushes the anterior tongue mass out of the mouth. This function requires sufficient axial stiffness to prevent buckling of the posterior tongue portion in combination with longitudinal compliance. In most squamates, these requirements are solved by the presence of an interior lingual process. Such stiff intrinsic structures are absent in snake tongues (Gnanamuthu, 1937; Langebartel, 1968), and a solution must be contained in the actively controlled soft tissue.

Two solutions may increase the axial stability of a muscular hydrostat: firstly, the incorporation of longitudinal muscle fibres in the circumferential periphery of the tongue and, secondly, adding extrinsic support from neighbouring tissues. Both solutions seem to be present in the tongue. Dorsal longitudinal fibre bundles are present in the anterior portion of the tongue (Hershkovitz, 1941; Smith and Mackay, 1990). A combined activation of the longitudinal muscle fibres (dorsal fibre bundles and intrinsic mm. hyoglossi) with the transversal antagonists (m. transversus, m. verticalis and m. circularis) results in a higher stiffness of the anterior tongue portion. The increased longitudinal forces may explain the reduced strain of the anterior portion, relative to the posterior portion of the tongue.

In the posterior portion of the tongue, such longitudinal muscle fibres in the circumferential periphery are absent, while a high axial stiffness is required in this portion because of the acceleration of the anterior tongue mass during protrusion. Intrinsic axial stiffness of the posterior portion of the tongue by means of peripheral longitudinal muscle fibres potentially reduces the protrusion forces and, consequently, the forward acceleration of the tongue mass. This is in conflict with the demand on longitudinal compliance. We propose that the tongue sheet and adjacent tissue substitute, at least partly, for the function of an internal stiff entoglossal process. External support of the protruding tongue mass prevents buckling and simultaneously enables longitudinal compliance.

The outer sheet is fixed in the mouth floor and is stiffened by the trachea (McDowell, 1972) and envelopes the posterior portion of the tongue (Figs 1, 2). Contraction of the muscles in the mouth floor, e.g. the m. ceratomandibularis and the m. intermandibularis (Frazzetta, 1966; Langebartel, 1968; McDowell, 1972), increase the stiffness of the tongue sheet and, thus, the external environment of the posterior tongue portion. The folded structure of the sheet contributes to the longitudinal compliance of the posterior portion of the tongue. Only the outer sheathing is connected to the mouth floor. The inward fold inserts about halfway along the contracted tongue at the so-called distal sheathing (Figs 1, 2). Elongation of the posterior portion of the tongue results in the outward folding of the inner sheathing at the distal fold (Fig. 2). Thus, the folded structure functions as a lubricated lining for tongue protrusion and subsequent retraction. Adventitiously, the tongue sheet is fully unfolded at the maximum protrusion length (Fig. 2) and the stress–strain characteristics of the connective tissue will constrain further tongue elongation.

The external solution for axial stiffness of the posterior portion of the tongue is advantageous over the intrinsic solution in the anterior tongue portion because it reduces the longitudinal contracting forces and the effective tongue mass. This advantage is illustrated by the observed differences in posterior and anterior strains. The anterior outer portion is unsupported, i.e. the external stabilisation cannot be applied after protrusion out of the mouth. Sagittal asymmetry of the longitudinal muscle fibres is required to resist gravitational forces, and peripheral longitudinal muscle fibres are needed for

intrinsic stiffness against buckling and not the least for flicking. Quite interestingly, the muscular tentacular stalks in the squid *Loligo pealei* are mechanically supported by two of the eight arms in the initial rapid extension phase during prey capture (Kier and Van Leeuwen, 1997). Perhaps, not surprisingly for a very similar combination of functional demands (i.e. pushing and extreme elongation), extrinsic support also evolved here as the solution to prevent buckling.

Experimental support for the proposed mechanism of tongue protrusion

We assumed axial stability in the posterior portion of the tongue in combination with high compliance in the longitudinal direction as an important demand for tongue protrusion. This demand is supported by observations in each of the three analysed tongue flick clusters. (1) The highest accelerations are generated while the tongue is still within the mouth and supported by the tongue sheet: maximum tongue tip velocities were observed at the moment of initial tongue tip protrusion out of the mouth (Fig. 5). (2) The tongue tips make a double 'clapping' movement while leaving the mouth, which may indicate mechanical instability during the initial acceleration. (3) After the tongue body protrudes beyond the labia of the mouth, the protrusion velocity decreases (Fig. 5) and the unsupported tongue portion is not further accelerated. (4) The first tongue flick coincides with the maximum tongue length, after which an overall negative protrusion velocity is observed (Figs 5, 6). The negative acceleration results in a dynamic stability of the tongue.

The mechanism of tongue retraction

Tongue retraction may be regarded as the opposite of tongue protrusion with one major difference: during retraction, the tongue mass is pulled at instead of pushed. Retraction of the tongue mass inherently provides dynamic stability. The extrinsic part of the paired mm. hyoglossi is the only candidate muscle to retract the whole tongue mass, and the intrinsic part of the mm. hyoglossi to contract the tongue body (negative strain), anteriorly assisted by the longitudinal dorsal muscles as previously suggested and supported by EMG observations of the mm. hyoglossi of garter snakes (Meredith and Burghardt, 1978) and other tongue-flicking squamates (Smith, 1984; Herrel et al., 1998).

Reflection on the evolution of snake tongues

The reduction of the lingual process is supposed to be related to tongue translations in chemoreception (Bels et al., 1994) and coincides with the development of a tongue sheet in the anguimorpha and snakes (McDowell, 1972). Based on the importance of axial stability of the tongue during protrusion, we hypothesised about the stability function of the entoglossal process in squamates and the substitute role of the tongue sheet for the absence of an internal skeletal support in snakes.

Stability of the unsupported tongue may well be a primary demand in the squamate tongue, e.g. while drinking. This intrinsic stability requires the development of peripheral longitudinal muscle fibres in the anterior portion of the tongue. Modification of the peripheral muscle fibres subsequently enabled tongue flicking. This development is supported by flicking observations (Gove, 1979; Herrel et al., 1998) and coincides with morphological transformations in the anterior tongue portion (Smith and Mackay, 1990).

Several authors used the tongue to study the taxonomic relationship between snakes and (tongue-flicking) lizards. The classification was based on morphological (McDowell, 1972) and behavioural characters combined with kinematics (Gove, 1979), the specialisation of the tongue towards chemoreception (e.g. Bels et al., 1994; Kardong et al., 1997) and morphological characters combined with kinematics (Smith and Mackay, 1990; Herrel et al., 1998). We cannot contribute to this discussion with our limited number of observations.

However, the externally observed tongue flicking is the result of 'behavioural' constraints on spatial and temporal tongue exposure, biomechanical interactions of constrained muscle dynamics and tongue inertia, and 'evolutionary' constraints in the inherited morphological and neurological characters. These characters are therefore dependent and should be analysed in an integrated manner. One means to study combined morphological characters and physiological constraints is the forward dynamic model simulation (e.g. Van Leeuwen, 2002). The predicted kinematics should agree with the quantitative findings presented here. The simulations will give insight into the mechanics and control of tongue flicking and will give supplementary support for the present plausible hypotheses on tongue protrusion and tongue flicking. By comparing predicted optimal solutions with actual solutions found in nature, a better understanding can be gained of the causal factors in the evolution of the tongue.

References

Bels, V. L., Chardon, M. and Kardong, K. V. (1994). Biomechanics of the hyolingual system in *Squamata*. *Adv. Comp. Env. Phys.* **18**, 196-240.

Bertmar, G. (1981). Evolution of vomeronasal organs in vertebrates. *Evolution* **35**, 359-366.

Chiel, H. J., Crago, P., Mansour, J. M. and Hathi, K. (1992). Biomechanics of a muscular hydrostat: a model of lapping by a reptilian tongue. *Biol. Cybern.* **67**, 403-415.

Chiszar, D., Scudder, K. M. and Knight, L. (1976). Rate of tongue flicking by garter snakes (*Thamnophis radix haydeni*) and rattlesnakes (*Crotalus v. viridis, Sistrurus catenatus tergeminus,* and *Sistrurus catenatus edwardsi*) during prolonged exposure to food odors. *Behav. Biol.* **18**, 273-283.

Chiszar, D., Radcliffe, C. W. and Scudder, K. M. (1977). Analysis of the behavioural sequence emitted by rattlesnakes during feeding episodes. *Behav. Biol.* **21**, 418-425.

de Groot, J. H. and Van Leeuwen, J. L. (2002). Estimation of the longitudinal axis of line symmetrical soft bodies by stereophotogrammetry. *J. Biomech.* **35**, 823-827.

de Groot, J. H. and Van Leeuwen, J. L. (in press). Evidence for an elastic projection mechanism in the chameleon tongue. *Proc. Roy. Soc. B.*

Frazzetta, T. H. (1966). Studies on the morphology and function of the skull in Boidae (Serpentes). Part II. Morphology and function of the jaw apparatus in *Python sebae* and *Python molurus*. *J. Morph.* **118**, 217-296.

Gillingham, J. C. and Clark, D. L. (1981). Snake tongue-flicking: transfer mechanics to Jacobson's organ. *Can. J. Zool.* **59**, 1651-1657.

Gnanamuthu, C. P. (1937). Comparative study of the hyoid and tongue of some typical genera of reptiles. *Proc. Zool. Soc. Ser. B* **107**, 1-63.

Gove, D. (1979). A comparative study of snake and lizard tongue-flicking, with an evolutionary hypothesis. *Z. Tierpsych.* **51**, 58-76.

Graves, B. M. and Halpern, M. (1990). Roles of vomeronasal organ chemoreception in tongue flicking, exploratory and feeding behaviour in the lizard, *Chalcides ocellatus*. *Anim. Behav.* **39**, 692-698.

Herrel, A., Timmermans, J. P. and De Vree, F. (1998). Tongue flicking in Agamid lizards: morphology, kinematics, and muscle activity patterns. *Anat. Rec.* **252**, 102-116.

Herrel, A., Meyers, J. J., Aerts, P. and Nishikawa, K. C. (2000). The mechanism of prey prehension in chameleons. *J. Exp. Biol.* **203**, 3255-3263.

Hershkowitz, J. (1941). On the finer structure of the tongue of *Lichanura roseofusca*. *J. Morph.* **68**, 71-80.

Kardong, K. V., Kiene, T. L. and Bels, V. (1997). Evolution of trophic systems in squamates. *Neth. J. Zool.* **47**, 411-427.

Kier, W. M. and Smith, K. K. (1985). Tongues, tentacles and truncs: the biomechanics of movement in muscular hydrostats. *Zool. J. Lin. Soc.* **83**, 307-324.

Kier, W. M. and Van Leeuwen, J. L. (1997). A kinematic analysis of tentacle extension in the squid *Loligo pealei*. *J. Exp. Biol.* **200**, 41-53.

Langebartel, D. A. (1968). The hyoid and its associated muscles in snakes. In *Illinois Biological Monographs* (ed. R. S. Bader, J. E. Heath, R. B. Selander, H. M. Smith and R. S. Wolfe), pp. 1-88. Urbania, Chicago, London: University of Illinois Press.

McDowell, S. B. (1972). The evolution of the tongue of snakes, and its bearing on snake origin. In *Evolutionary Biology*, vol. 6 (ed. T. Dobzhansky, M. K. Hecht and W. C. Steere), pp. 191-273. New York: Appleton-Century-Crofts.

Meredith, M. and Burghardt, G. M. (1978). Electrophysiological studies of the tongue and accessory olfactory bulb in garter snakes. *Phys. Behav.* **21**, 1001-1008.

Schwenk, K. (1994). Why snakes have forked tongues. *Science* **263**, 1573-1577.

Schwenk, K. (1995). Of tongues and noses: chemoreception in lizards and snakes. *Trends Ecol. Evol.* **11**, 7-11.

Smith, K. K. (1984). The use of the tongue and the hyoid apparatus during feeding in lizards (*Ctenosaura similis* and *Tupinambis nigropunctatus*). *Zool. Lond.* **202**, 116-143.

Smith, K. K. (1986). Morphology and function of the tongue and the hyoid apparatus in *Varanus* (Varanidae, Lacertilia). *J. Morph.* **187**, 261-287.

Smith, K. K. and Mackay, K. A. (1990). The morphology of the intrinsic tongue musculature in snakes (Reptilia, Ophidia): functional and phylogenetic implications. *J. Morph.* **205**, 307-324.

Smith, K. K. and Kier, W. M. (1989). Trunks, tongues and tentacles: moving with skeletons of muscle. *Am. Sci.* **77**, 28-35.

Snelderwaard, P. Ch., de Groot, J. H. and Deban, S. M. (2002). Digital video combined with conventional radiography creates an excellent high-speed X-ray video system. *J. Biomech.* **35**, 1007-1009.

Ulinski, P. S. (1972). Tongue movements in the common boa (*Constrictor constrictor*). *Anim. Behav.* **20**, 373-382.

Van der Helm, F. C. T., Veeger, H. E. J., Pronk, G. M., Van der Woude, L. H. V. and Rozendal, R. H. (1992). Geometry parameters for musculoskeletal modelling of the shoulder mechanism. *J. Biomech.* **25**, 129-144.

Van Leeuwen, J. L. (2002). Tongues and tentacles: modelling and optimization of protrusible muscular systems. *Comp. Bioch. Physiol. A* **132**, S82-S83.

Van Leeuwen, J. L. and Kier, W. M. (1997). Functional design of tentacles in squid: linking sarcomere ultrastructure to gross morphological dynamics. *Phil. Trans. R. Soc. B* **352**, 551-571.

Van Leeuwen, J. L., de Groot, J. H. and Kier, W. M. (2000). Evolutionary mechanics of protrusible tentacles and tongues. *Neth. J. Zool.* **50**, 113-139.

Woltring, H. J. and Huiskes, R. (1990). Stereophotogrammetry. In *Biomechanics of Human Movement* (ed. N. Berme and A. Cappozzo), pp. 108-127. Worthington, Ohio: Bertec Corporation.

Young, B. A. (1990). Is there a direct link between the ophidian tongue and the Jacobson's organ? *Amphib. Rept.* **11**, 263-276.